

ARTICLE OPEN



Spider-inspired tunable mechanosensor for biomedical applications

Taewi Kim^{1,8}, Insic Hong^{1,8}, Yeonwook Roh^{1,8}, Dongjin Kim¹, Sungwook Kim², Sunghoon Im¹, Changhwan Kim¹, Kiwon Jang¹, Seongyeon Kim¹, Minho Kim¹, Jieun Park¹, Dohyeon Gong¹, Kihyeon Ahn¹, Jingoo Lee¹, Gunhee Lee³, Hak-Seung Lee⁴, Jeehoon Kang⁴, Ji Man Hong⁵, Seungchul Lee², Sungchul Seo⁶, Bon-Kwon Koo^{1,7}, Je-sung Koh¹, Seungyong Han¹ and Daeshik Kang¹

The recent advances of wearable sensors are remarkable but there are still limitations that they need to be refabricated to tune the sensor for target signal. However, biological sensory systems have the inherent potential to adjust their sensitivity according to the external environment, allowing for a broad and enhanced detection. Here, we developed a Tunable, Ultrasensitive, Nature-inspired, Epidermal Sensor (TUNES) that the strain sensitivity was dramatically increased (GF ~30k) and the pressure sensitivity could be tuned (10–254 kPa⁻¹) by preset membrane tension. The sensor adjusts the sensitivity to the pressure regime by preset tension, so it can measure a wide range (0.05 Pa–25 kPa) with the best performance: from very small signals such as minute pulse to relatively large signals such as muscle contraction and respiration. We verified its capabilities as a wearable health monitoring system by clinical trial comparing with pressure wire which is considered the current gold standard of blood pressure ($r = 0.96$) and home health care system by binary classification of Old's/Young's pulse waves via machine learning (accuracy 95%).

npj Flexible Electronics (2023)7:12; <https://doi.org/10.1038/s41528-023-00247-2>

INTRODUCTION

Spiders have not only extremely high sensitivity but also an astonishing ability to modulate the sensitivity of the sensory organs by lowering the threshold for external signals that compression/tensile stress acting on the sensory organs through changing the leg posture^{1,2}. A spider's slit organ, a strain sensory organ, detects physical deformation or strain. They form narrow (width 1–2 μm) elongated slits with thin (0.25 μm) covering membrane sensory cells attaches³ (Supplementary Fig. 1). The sensory cells transduce mechanical stimulation to the neural firing rate⁴. The range of neural firing rate limits the range and resolution of the spider's sensation. However, spiders seem to overcome the limitations by adjusting their sensitivity by varying the position of the leg. Their slit sensory organs became insensitive in the leg close state and sensitive in the extension state, a difference of 224 times³. Many researchers have paid attention to the potential to tune their sensitivity according to the external environment in other biological sensory systems that allow wide-ranging and enhanced detection^{2,5}. Meanwhile, the remarkable advances in mechanosensory of the capability to measure strain^{6,7}, pressure^{8–10}, and vibration¹¹ have enabled miniaturization, ultrahigh sensitivity^{12,13}, omnidirectional detection¹⁴, flexibility, and even stretchability of devices^{15,16}. Specifically, nanoscale crack-based electrodes⁷, anisotropically resistive structure¹⁷, and microstructured dielectric/electrode structure⁹ contribute to ultra-sensitivity. Also, intrinsically stretchable materials for electrode/substrate¹⁸, serpentine patterns¹⁹, and kirigami designs²⁰ improve the stretchability and sensing range. In particular, combined with a skin-attachable form factor, epidermal sensors have been developed to enable precise bio-signal measurement with minimized stimulation at the skin interface,

such as nanomesh-based breathable electronics²¹ and wireless vital signal monitoring system²². In addition, epidermal electronics expand its application to tactile sensors integrated with actuators for virtual and augmented reality²³ and deep learning technology to minimize the number of sensors for precise motion tracking²⁴.

However, each sensor has a tradeoff relationship between measurement range and sensitivity. For example, a broad measurement range causes the low sensitivity, and on the other hand, high sensitivity reduces the detectable range of the sensor. It causes that different sensors must be used depending on the target signal (Supplementary Fig. 2). This conflicting relationship occurs due to physical limitations in the signal processing, and similar limitations exist in nature, such as action potential firing rate. The nervous system converts physical stimuli into electrochemical signals called action potentials and transmits them to the brain. Action potentials arise from changes in the membrane potential caused by ion transport across cell membranes, and voltage fluctuations often take the form of rapid rising spikes and rapid drops. As the magnitude of the stimulus increases, the action potential appears at a faster frequency without changing the magnitude. Because there is a physical limit to the resolution and frequency range of this action potential²⁵, sensitive receptors have a small detection range. Since spiders have very sensitive strain sensing organs, it can be difficult to discriminate against large stimuli, but this limitation is overcome by actively adjusting the sensitivity according to the leg posture. Here, we developed and demonstrated Tunable, Ultrasensitive, Nature-inspired, Epidermal Sensor (TUNES) that mechanosensors inspired by spider's sensory systems can easily adjust their sensitivity by preset strain—dramatically increased sensitivity for the pressure regime of the signal. The tunability arises from the nonlinear characteristics of

¹Department of Mechanical Engineering, Ajou University, Suwon, Korea. ²Department of Mechanical Engineering, Pohang University of Science and Technology, Pohang, Korea. ³Department of Sustainable Environment Research, Korea Institute of Machinery & Materials, Daejeon, Korea. ⁴Department of Internal Medicine and Cardiovascular Center, Seoul National University Hospital, Seoul, Korea. ⁵Department of Neurology and Neurosurgery, Ajou University School of Medicine, Suwon, Korea. ⁶Department of Nano-chemical, Biological and Environmental Engineering, Seokyeong University, Seoul, Korea. ⁷Institute on Aging, Seoul National University, Seoul, Korea. ⁸These authors contributed equally: Taewi Kim, Insic Hong, Yeonwook Roh. ✉email: bkoo@snu.ac.kr; jskoh@ajou.ac.kr; sy84han@ajou.ac.kr; dkang@ajou.ac.kr

the nanoscale-crack-based sensor used. Thus, our single sensor can measure diverse biosignals such as respiration, muscle contraction/relaxation, and minute wrist pulse and presented the potential of biomedical application through comparison with a commercial medical device in a clinical trial. Furthermore, we have shown that our sensor can be used to diagnose and monitor human health in the future by classifying pulse signals from the Young and Old groups through machine learning.

RESULTS

Spider leg joint inspired-tunable sensor to detect broad dynamic range

The mechanism of the spider and our sensor's tuning sensitivity is illustrated in Fig. 1, respectively. In the spider, strain detectors consisting of parallel slits embedded in cuticles and covered by an outer membrane are located near the leg joint (Fig. 1a, b). Slits in leg are compressed or released along the leg posture, as shown in Fig. 1c, and vibration from external force closes the slit with compression (Fig. 1d). The extended leg with a more compressed slit can amplify the organ sensitivity by shifting the threshold¹ (Fig. 1e). The changed sensitivity in the slit can allow the spider to detect various vibration from high to low magnitudes for having captured small prey or escaping from huge predators (Fig. 1f). By mimicking the geometry and tuning mechanism of the slit organ, we designed a sensor with a nonlinear variance of resistance to applied strain⁷ by generating nanoscale cracks on a metalized polyimide (PI) film²⁶ (Fig. 1g). The thickness of the sensor was only ~10 μm which enabled it to be ultralight in weight (~6 mg) and flexible (Fig. 1h). The generated cracks by tensile stress were straight and perpendicularly aligned to the tensile direction (Fig. 1i, j). The sensing mechanism of the crack sensor is compressing and releasing nano-scale cracks (Fig. 1k). Also, as shown in Fig. 1l, m, the crack sensor can adjust the sensitivity via pre-strain to the sensor (Preset strain: 0–1%) as with the spider leg. Tunable sensitivity of the sensor enables the adjustable dynamic range that allows the sensor to monitor strain and pressure of various scale with a single sensor.

Characteristic of a tunable crack sensor according to preset strain

The fabricated crack sensor has a capability to adjust its sensitivity to measure strain or pressure of various range. We designed a tensile test using the crack sensor and uniaxial stretcher, as shown in the experimental setup (Supplementary Fig. 3a), to confirm sensitivity and measurable range of the crack sensor according to preset strain (0, 0.5, and 1%). A key feature to arrange sensitivity of the crack sensor is the nonlinear characteristics that cause to dramatically increase resistance as the tension increases at the nanoscale crack. When a tensile test machine (3342 UTM, Instron Co.) stretches at 0.5, 1, 2% and releases to initial state, the strain sensitivity reaches up to gauge factor (GF) of 1.3 k, 12.7 k, 30 k at 0.5, 1, 2% strain, respectively, while the GF is defined as $\Delta R/(eR_0)$ where e is applied strain and R_0 is base resistance (Supplementary Fig. 3b). Theoretical modeling and simulation for crack-based sensor are provided in Supplementary Note 1 and Supplementary Fig. 4. A further tension in the crack, however, causes an irreversible disconnection, because of plastic deformation of the substrate of the crack sensor at above 2%. These results indicate the intrinsic range depending on set sensitivity. For example, the measurable strain range with preset at 0, 0.5, and 1% is, respectively, 0.00167–2%, 0.000133–1.5%, and 0.0001–1.1% (Supplementary Fig. 3c).

We also fixed, as the former test, our sensor to the uniaxial stretcher and set up non-preset and presets at 0.5, 1% to confirm the possibility of tunable pressure sensitivity in the sensor (Fig. 2a). As shown in Supplementary Fig. 5, our sensor has ability to detect

minute vibration by tuning fork test. Also, large variations in resistance were obtained by pressure, applied to the opposite side of deposited metal layers, up to 25 kPa (Fig. 2b); at 11 kPa, the pressure sensitivity upon application of a 1% preset strain was fivefold higher than that when no pressure was applied (Fig. 2c). FEA simulation was conducted to verify mechanical deformation against pressure when the crack-based sensor was pre-strained, showing a uniform strain applied across the sensor and linear increase of strain with respect to the preset strain and applied pressure (Supplementary Fig. 6).

The results indicate that due to the sensor characteristics, pressure sensitivity ($S = dR/dP$, where R is resistance and P is applied pressure) can be tuned by setting the initial tension. Figure 2d shows the static response of the sensor under a 2 kPa pressure applied at a speed of 20 mm/min for 10 s. The resistance responses were 26, 63, and 100 Ω, when the preset strains were 0, 0.5, and 1%, respectively, and the resistance was maintained within 2%, as forces were applied. Here, dynamic ranges for pressure after each preset at 0, 0.5, and 1% are 10–25 kPa, 2.5–17 kPa, and 0.05–12 kPa (Fig. 2e). The minimum and maximum pressure were measured based on a value that satisfies the pressure sensitivity of 50 kPa⁻¹ or more and a value in which the baseline of the sensor does not change. The dynamic response and durability of our device were verified by applying a 2 kPa pressure for 10,000 cycles (Fig. 2f). The two inset graphs at the bottom of Fig. 2f showing the resistance responses after 2000 and 8000 cycles reveal that a lower preset strain results in higher durability (2.4 and 1.3 % sensitivity drop with and without, respectively, a 1% preset strain). As an outstanding of TUNES compared with previous studies^{10,27–36}, the conventional pressure sensors require compromise of the sensor characteristics, in which the sensitivity decreases as the measurement range increases or low sensitivity over a wide pressure range (Fig. 2g, h). On the other hand, since TUNES can optimize sensitivity through preset strain control, it not only maintains high sensitivity when detecting high pressure, but also significantly improves the limitations of piezoresistive sensors that should be fabricated for the optimized sensor's sensitivity. These results present that adjustable sensitivity and measurable range via preset strain are key properties to measure various mechanical signals with utmost performance. The performance of existing piezoresistive flexible and epidermal pressure sensors in terms of structures, materials, sensitivity, min detection limit, tunability, and thickness is summarized in Supplementary table 1.

Tunable mechanosensory system to monitor vital signals of a broad range

To demonstrate the capability of TUNES to monitor mechanical bio-signals which have various pressure regime as medical application, we applied TUNES to human body that yields biological signals such as ribcage, arms, and wrist. As shown in Fig. 3a, we design the TUNES, controlling the preset strain of the sensor and tuning its sensitivity according to the subject's signal amplitude to monitor vital signals. The thin film type crack-based strain sensor was assembled with strain–pressure transducer to measure pressure. Both sensor ends were fixed to the transducer, which is adjustable spacing to exert the present strain (0–1%) for tuning sensitivity of the sensor. Figure 3b illustrates characteristics of our TUNES. The widened cracks by the preset strain have more sensitive to strain because the resistance increases along the quadratic curve as the gap widens. More details of fabrication and sensitivity control of TUNES are provided in Supplementary Methods and Supplementary Note 2.

When a person inhales, the intercostal muscles contract to increase the anteroposterior diameter of the ribcage (called the pump handle movement)³⁷. TUNES (Preset: 0%, 0.5%), tightened with a flexible band as shown in Fig. 3c, and flow meter as

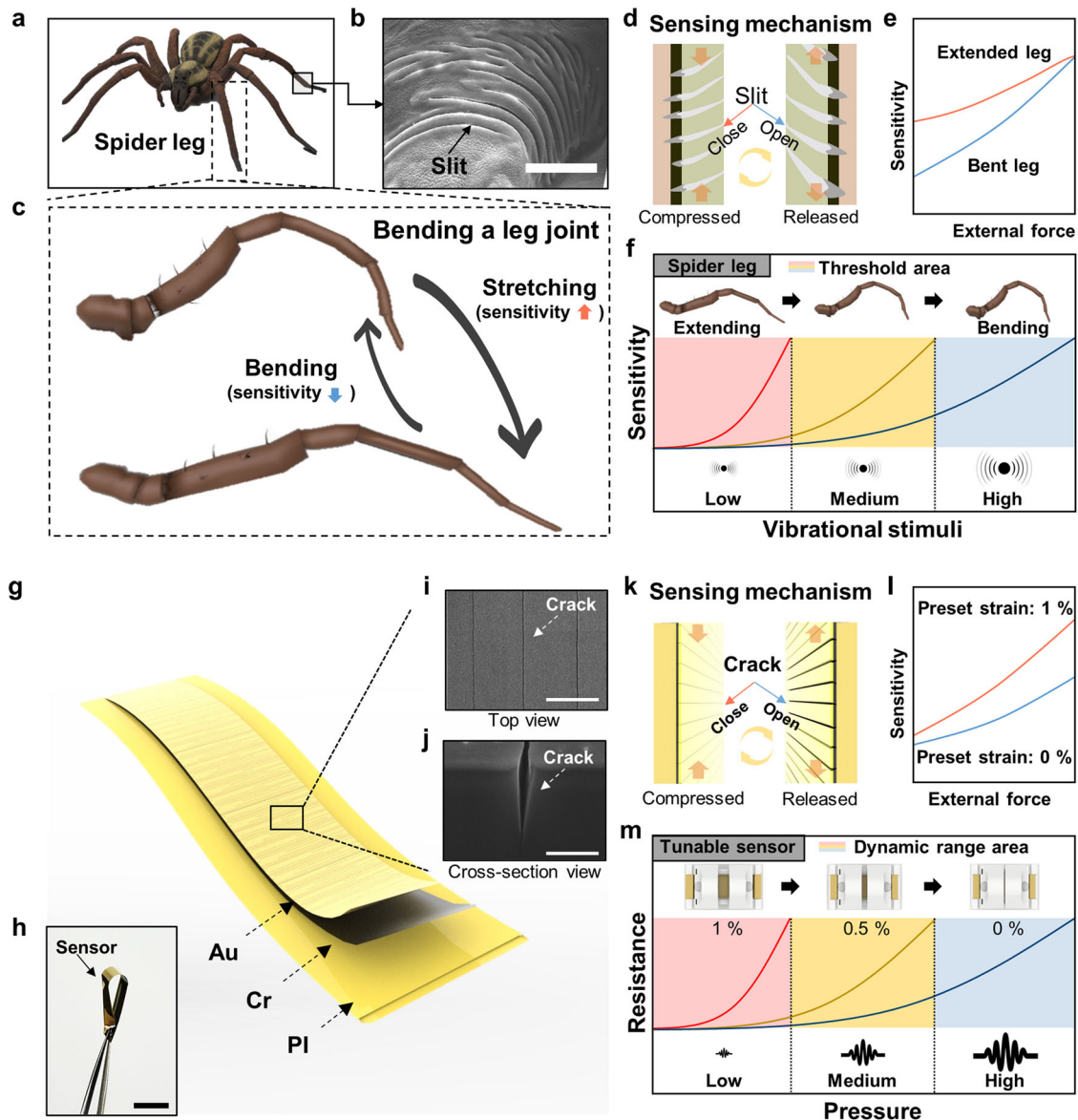


Fig. 1 Sensitivity tuning mechanism inspired by the sensory organs of spiders. **a** Schematic illustration of a wandering spider. **b, c** The spider's leg is an active substrate that can modulate the intensity of stimulation according to the tension acting on the end organ with slit (Scale bar: 30 μm). **d** Schematic illustration of the morphological features of the slit organ along heavier of a leg joint. **e** Comparison of the sensitivity of spider leg depending on open and close of slit. **f** Schematic of the spider's sensitivity tuning mechanism: Sensitivity is increased by lowering the threshold of the sensory organs when the leg of spider is bent. **g** Schematic illustration of the crack-based strain sensor consisting. **h** Photograph of the flexible crack sensor (Scale bar: 1 cm). **i** Top view of an SEM image of a crack on the conductive layer (Scale bar: 3 μm). **j** Cross-sectional SEM image of a crack penetrating into the PI layer (Scale bar: 500 nm). **k** Schematic illustration of the morphological feature of the crack sensor along strain. **l** Comparison of the sensitivity of the crack sensor along the open and close of the crack. **m** Adjusted dynamic range of the crack sensor by pre-set strain.

reference device, monitored respiration which varied with the changing volume of the chest cavity. When monitoring respiration with deep pressure via preset 0%, the results from TUNES matched the data from flow meter without any noticeable difference (Fig. 3d). Preset 0.5% in TUNES, on the other hand, caused excessive strain to the sensor with the irreversible damage (Fig. 3e). Another application of TUNES is monitoring contraction and relaxation of muscle as electromyography (EMG). When muscle contracts, changes in volume, cross-sectional area,³⁸ and hardness³⁹ occur that change the pressure on a sensor attached to the skin. We attached our sensor with 0.5 and 1% of preset strain and EMG electrodes to a bicep of a test subject and simultaneously measured the signals as the subject lifted a dumbbell (Fig. 3f and Supplementary Movie 1). The magnitude and shape of

the electrical signal, measured by the EMG sensor, were similar to our sensor response in the former preset (Fig. 3g), showing us the possibility of detecting elbow flexion or muscle contraction using our sensor. The latter preset in the TUNES, however, was not suitable to monitor the muscle contraction and expansion because of the excessive preset strain (Fig. 3h). Although the radial pulse originating from the wrist is a minute signal, monitoring of the radial pulse can briefly check the heart rate. In the case of detecting pulse wave as shown in Fig. 3i, TUNES needs to amplify the obtained signals through high sensitivity using maximum preset (1%) and monitored enlarged pulse of the wrist (Fig. 3j), whereas minimum preset, as shown in Fig. 3k, displayed elusive signals of small amplitude. The detail of

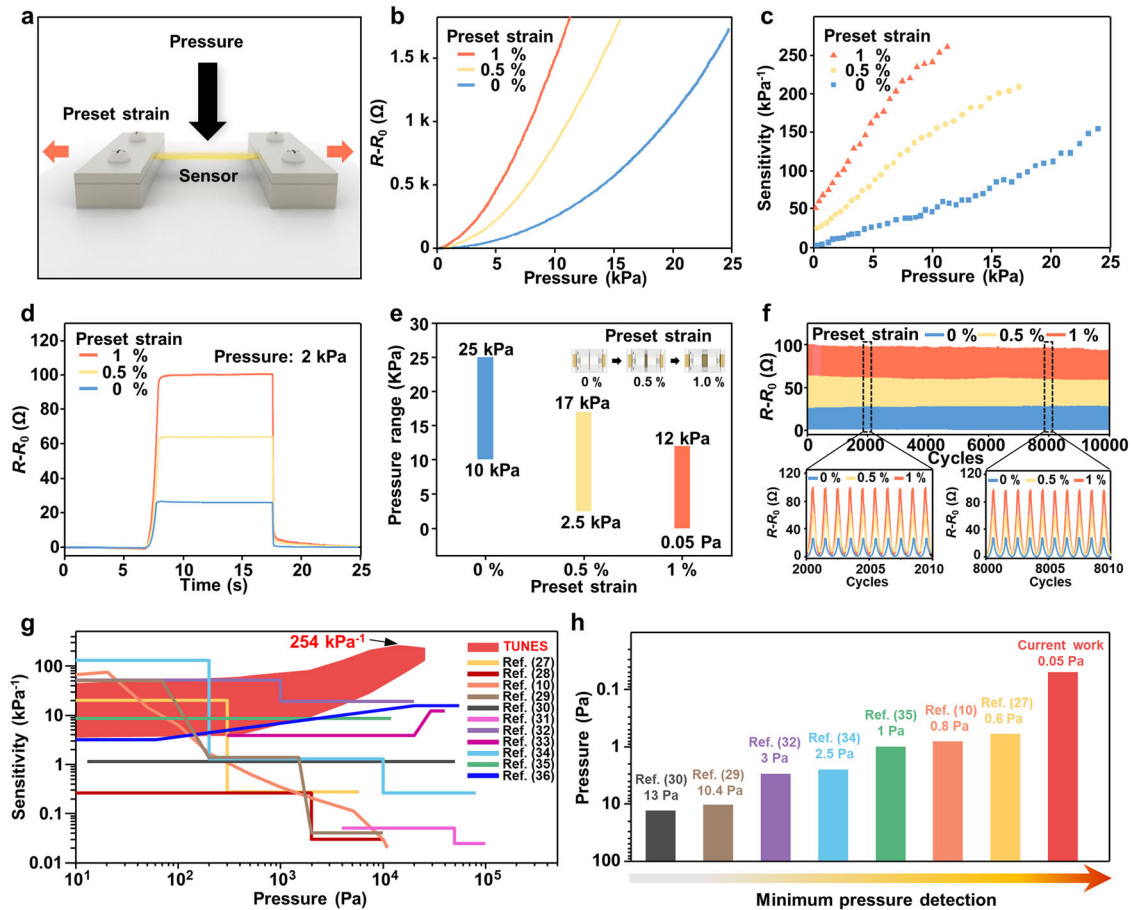


Fig. 2 Tunable sensitivity and mechanical characterization of the crack sensor. **a** Schematic of the experimental setup for pressure sensing with preset strains of 0, 0.5, and 1%. **b** The vertical displacement–pressure curve while applied strain was 0, 0.5, and 1%. **c** Resistance response of the sensor according to the applied pressure with preset strain. **d** Resistance response of the sensor with a preset strain at 2 kPa pressure. **e** Pressure range determined by preset strain. **f** Resistance response of the sensor with preset strain over 10,000 cycles of loading at 2 kPa pressure (cycles 2000–2010, left, and cycles 8000–8010, right, are shown in expanded views below). **g** Pressure sensitivity comparison in detectable pressure range (Maximum sensitivity and pressure range was reached up to 254 kPa^{-1} and $\sim 25 \text{ kPa}$, respectively at this work). **h** Performance comparison of minimum detectable pressure (TUNES could detect $< 0.05 \text{ Pa}$ range).

experimental testing methods is provided in Supplementary Note 3 and Supplementary Figs. 8, 9, 10, and 11.

TUNES for a non-invasive biomedical sensor

For numerous wearable sensors, pulse wave measurement has been used as an application until now, but their accuracy was unverified or too low to put to practical use. Having demonstrated the tunability of our sensor, we then evaluated the accurate, noninvasive, and continuous measurement of pulse waves that is a critical bio-signal to indicate cardiac performance, vascular age, and sympathovagal interaction as wearable device. We designed a strain-controllable frame that can monitor the various vital signals on the skin as detailed in precedent session (Fig. 4a). The enhanced sensitivity of the device allowed us to perform the measurements at various pulse points on the body. The pulse wave velocity (PWV) and pulse transient time (PTT) could be measurable by simultaneously monitored by electrocardiography (Supplementary Fig. 12) that is generally considered to be a promising technique for noninvasive continuous blood pressure measurements⁴⁰. We also evaluated the accuracy and reliability of the sensor through clinical trials by comparing it with pressure wire which is considered the current gold standard of intravascular blood pressure⁴¹. The trials were conducted in a controlled operating theater (Supplementary Fig. 13) at the Cardiovascular Center of the Seoul National University Hospital (Fig. 4b), and the

sensor was secured using medical tape to the skin above the right brachial artery of the subject; the inset photograph in Fig. 4b shows the catheter and pressure wire (PW) inserted into the artery (Supplementary Fig. 14). Figure 4c shows an X-ray image of the intravascular PW and the wired part of the sensor; the PW was inserted through the radial artery, and the pulse was measured at the brachial artery, where the sensor was located. Figure 4d shows a graph comparing the invasive blood pressure (IBP) signal measured through the catheter and PW and the noninvasive signal obtained simultaneously with our sensor. Because the IBP through the catheter was measured in the radial artery, the graph shape and blood pressure magnitude slightly differed from those obtained when the IBP was measured through the PW (a similar waveform was obtained when the sensor was attached to the opposite radial artery; Supplementary Fig. 15). However, our sensor placed at the same position was correctly calibrated with the PW (Fig. 4e). The Pearson correlation coefficient between the data from the PW and those from our sensor matched with each other and was 0.96, which indicates that the two data are corresponded (Supplementary Fig. 16). The pulse wave calibrated with blood pressure could be used for non-invasive continuous monitoring of hemodynamic parameters, such as cardiac output and stroke volume, which are useful for the intensive care of seriously ill patients⁴² (Supplementary Figs. 17 and 18). Further

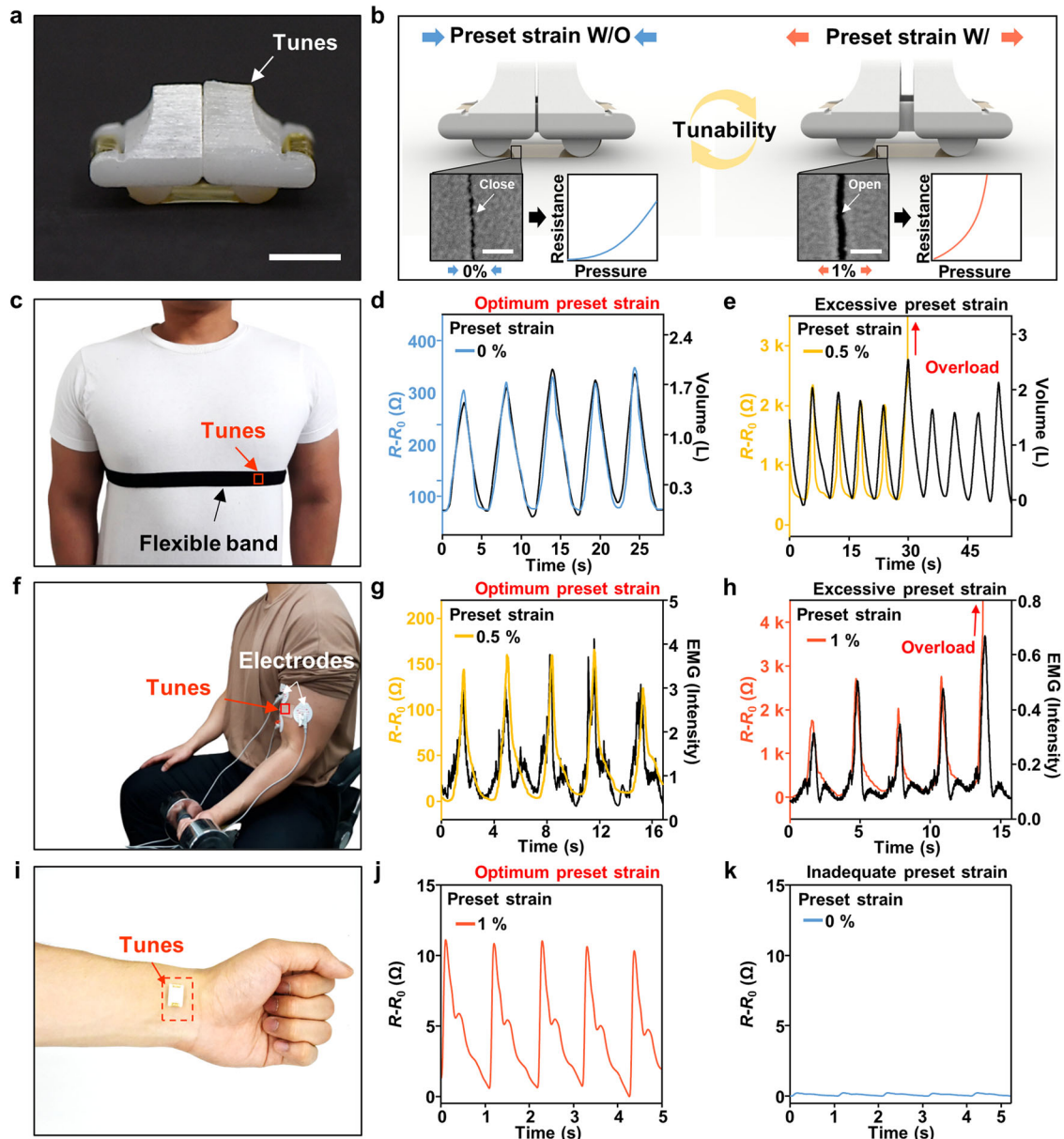


Fig. 3 Precise pulse wave measurement by TUNES. **a** Photograph of the TUNES (Scale bar: 0.5 cm). **b** Schematic illustration of the TUNES adjusting the preset to match measured range with control of the crack gap (Scale bar: 300 nm). **c** Photograph of measuring respiration by TUNES. **d, e** Comparison of respiration through the optimum (0%) and excessive (0.5%) preset of TUNES. **f** Photograph of measuring muscle signals via TUNES and EMG sensor. **g, h** Comparison of EMG through the optimum (0.5%) and excessive (1%) preset of TUNES. **i** Photograph of TUNES attached to radial artery. **j, k** Measured pulse wave of radial artery measurement by TUNES with preset strain 1 and 0%.

information on measurements at various pulse points on the body can be found in Supplementary Note 4.

Other potential applications of our tunable sensor are analysis of stress in daily life and cardiac performance examinations. Heart rate variability (HRV)—the number of fluctuations around the mean heart rate—is a valuable measure of the sympathetic and parasympathetic functions of the autonomic nervous system and can also be used for stress analysis⁴³. We evaluated that the high accuracy and wearability of TUNES can extend HRV analysis to various physical activities. As shown in Supplementary Fig. 19a, attaching the sensor to the skin above the superficial temporal artery, next to the ear, minimizes the noise caused by joint movements and enables precise HRV measurements, even during daily life activities such as cycling (Supplementary Movie 2). The HRV tachogram was recorded in three different conditions: sleeping, sitting, and cycling for 10 min (Supplementary Fig. 19b). In each

condition, the pulse wave was measured with high accuracy and very little noise (Supplementary Fig. 20). In addition, the histogram, Poincare plot, and power spectral density (PSD), which are important indicators of HRV, were very reasonable (Supplementary Fig. 19c–e). We also conducted a cardiac stress test using the Balke protocol⁴⁴ that the body movement was very active (Supplementary Fig. 19f). As shown in Supplementary Fig. 19g, the pulse wave could be monitored while the subject walked on a treadmill which increases the incline by 1% every minute. Supplementary Fig. 19h, i shows the pulse wave measured 1 min after the test was started and at the highest heart rate (after 15 min). In each moment, the waveforms contained three major peaks (Supplementary Fig. 21). Furthermore, the enhanced sensitivity of the sensor could simplify and miniaturize the measurement device so that it enables in-home health management systems by using a smartphone in conjunction with wireless communication (a prototype setup is shown in

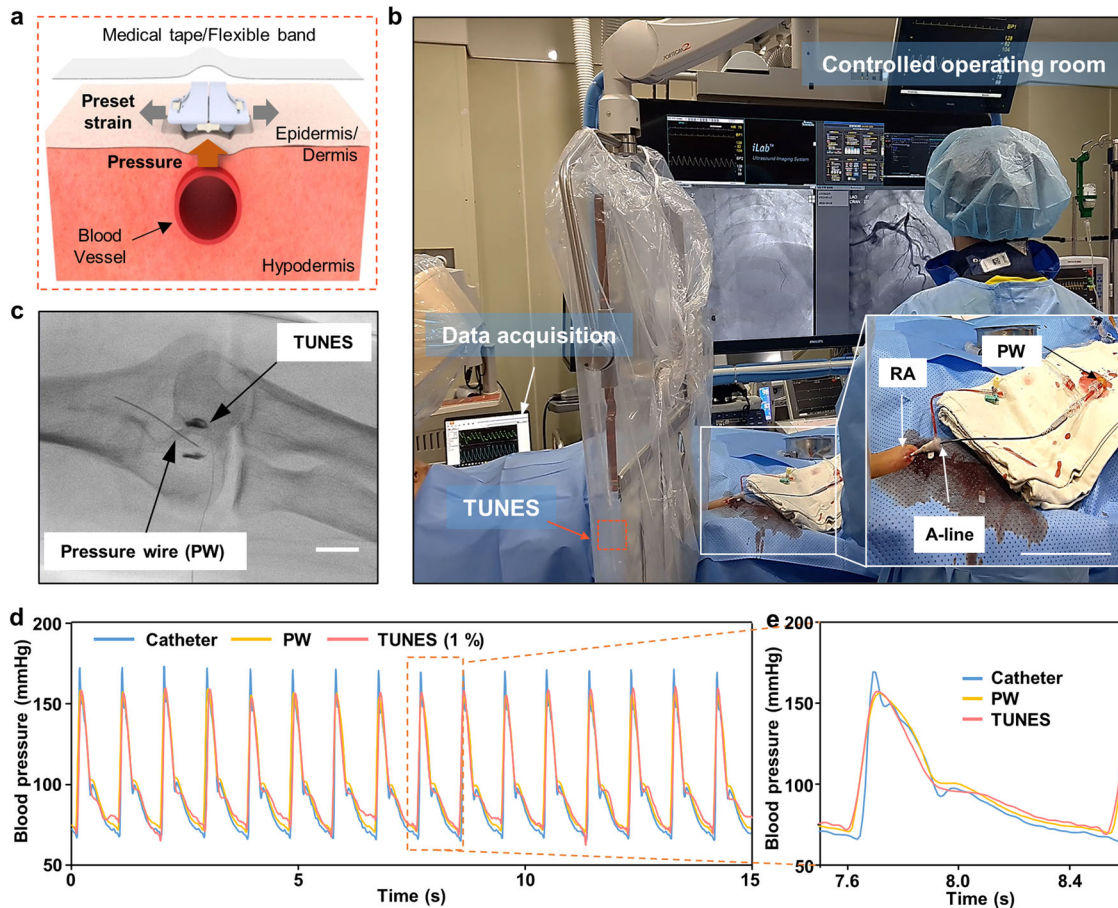


Fig. 4 The tunable sensor for a skin-attachable biomedical sensor. **a** Schematic of strain tunable frame for measuring pulses signal. **b** Digital photograph of the Controlled operating room. The lower right inserted image is a magnified white box (Scale bar: 5 cm). **c** X-ray image when the tunable sensor was attached to a brachial artery and the pressure wire passes through the artery (Scale bar: 1 cm). **d** Simultaneous measurement of invasive blood pressure monitoring systems (catheter and pressure wire) and the tunable sensor. **e** Magnified curves of dashed box at (d).

Supplementary Fig. 22 and Supplementary Movie 3). The detail of set up for wireless monitoring system is provided in Supplementary Note 5.

Classification of pulse wave through machine learning

The final goal of developing wearable healthcare sensors is to improve the user's health by diagnosing and predicting diseases. Currently, analyzing biological signals through machine learning is being actively conducted, but most of them are based on data measured in hospitals due to the inaccuracy of wearable sensor data. To demonstrate that the improved sensitivity of the sensor can help diagnose and predict cardiovascular disease by machine learning, we obtained a pulse wave dataset from two experimental groups that have different age and gender which are the most influential factors of pulse wave and used it as training data in a machine learning model for classification. One group, referred to as "Young", consisted of 21 men in their 20 s, and another, designated "Old", were 21 women in their 70 s. Machine learning often requires augmentation of the original data during the training phase to acquire a sufficient amount of data⁴⁵. For data augmentation, we split each dataset into several pieces, obtaining 3921 augmented data (Fig. 5a); Fig. 5b, c shows a single case from each group. Although the given figures were distinctive enough to represent the Young and Old groups, there were some outliers, thus allowing machine learning to play its role. We assigned labels 0 (Young) and 1 (Old) to every piece of pulse wave data. Then, we applied signal processing principles to better distinguish the two

groups based on the pulse wave data. In the time domain, the notable features of a waveform signal include the mean, maximum, root mean square, skewness, kurtosis, kurtosis factor, crest factor, impulse factor, shape factor, margin factor, and peak-to-peak value (Fig. 5c). These 11 different features were combined with the previously augmented data together with the 0/1 assignment, giving a final matrix shape of 3921 by 12. Then, the dataset was input into random forest⁴⁶, which is a well-known high-performance machine learning classifier model (Fig. 5d). For the 1177 test data, we achieved a classification accuracy of up to 94.9 and 75% with and without, respectively, applying a 1% preset strain (Fig. 5e and Supplementary Fig. 23). As shown in the above results, the sensitivity of the sensor is a major factor in the future healthcare system using machine learning, and our sensor has shown its feasibility.

DISCUSSION

In summary, we developed an ultrasensitive tunable mechanosensor inspired by spider's slit organ that can tune its sensitivity by adjusting the preset strain. Compared to existing pressure sensors with conflicting between sensitivity and measurement range, our sensor has tunable sensitivity of 10–254 kPa⁻¹ under pressure regime of 0.05 Pa–25 kPa that enhances bio-signal detection of various pressure ranges. We have shown the feasibility that the enhanced bio-signal (especially pulse waves) can realize the wearable home-healthcare & self-diagnostic system

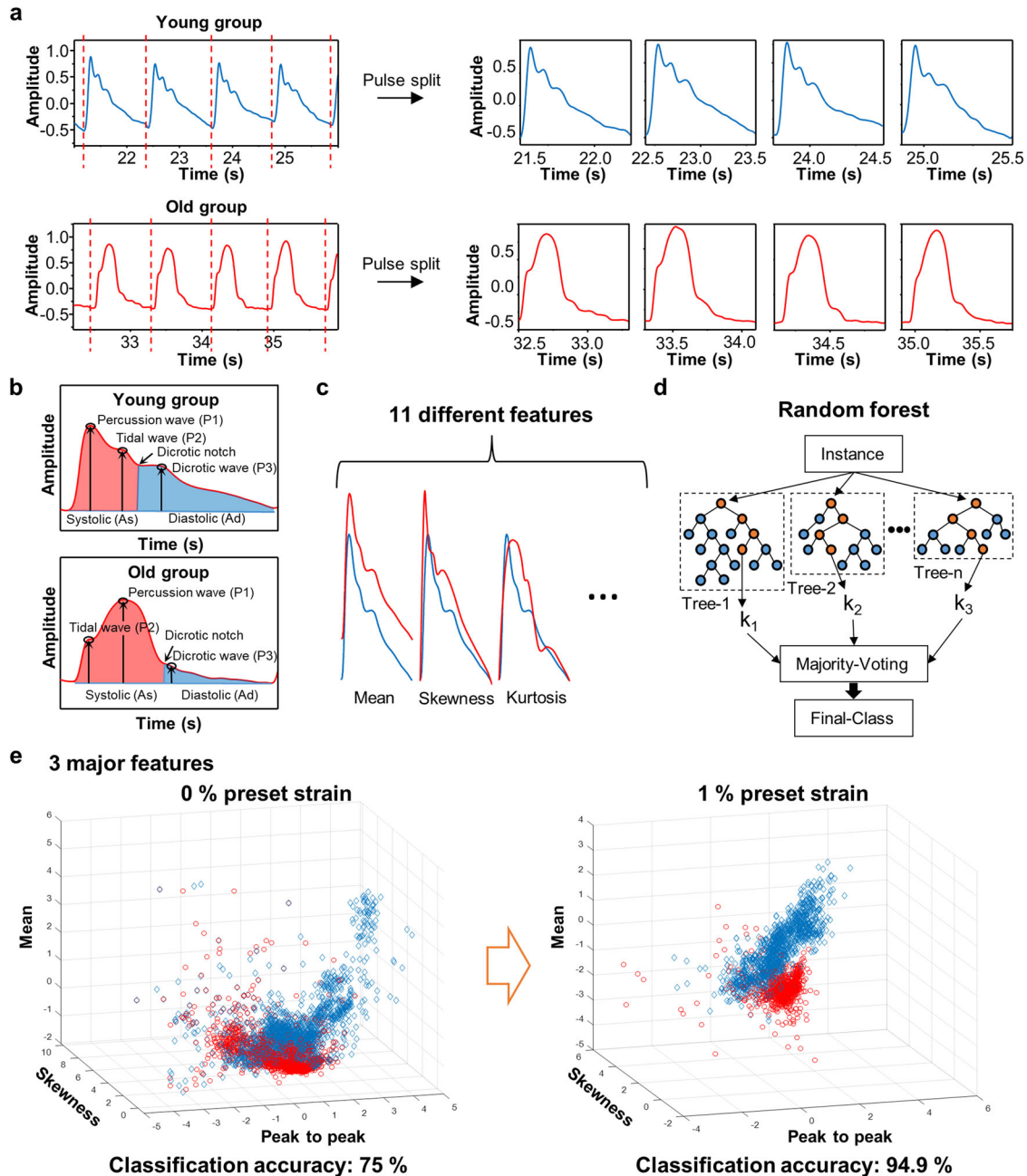


Fig. 5 Classification of pulse wave measured by TUNES with artificial intelligence. **a** Preprocessing of pulse wave data. **b** Characteristics of a pulse wave from a subject in the Young group and Old group. **c** Eleven different features were derived from the pulse signal. **d** Schematic illustration of the Random forest algorithm. **e** Random forest classification of pulse wave data. The classification rates were 94.9% with 1% preset strain and 75% without preset strain.

through non-invasive blood pressure monitoring and machine learning. The improved sensitivity provided high precision and resolution in pulse wave measurements. The similarity of the pulse wave between TUNES and an invasive blood pressure measurement (pressure wire) which is known as the gold standard was 96%. TUNES could measure the pulse wave at various pulse points, and we measured the temporal artery even in exercise states such as walking and cycling. In addition, the measurement & Bluetooth transmission system could be made up of a simple embedded circuit without large and complicated equipment. Future work focuses on the development of an integrated system that combines wireless communication with motor control systems to automatically control sensor's preset strain with optimal

sensitivity and improve structural flexibility of sensor based on the intrinsic stretchable materials or kirigami designs to detect a wider range of pressure without damage.

METHODS

Characterization of TUNES

We used field emission scanning electron microscopy (FE-SEM) (S-4300SE microscope, Hitachi Ltd., Tokyo, Japan) to analyze the behavior of nano-scale cracks. Strain controllable frame was fabricated by a 3D printer (ProJet MJP 2500, 3D SYSTEMS. Co., Rock Hill, SC, USA). A thermal evaporation system (Thermal Evaporation System, DD High Tech. Co., Gimpo-si, South Korea)

was used to sequentially deposit chromium, gold layer on the PI film (3022-5 Kapton thin film, Chemplex, Palm City, FL, USA). The crack sensor was stretched by a material testing machine (3342 UTM, Instron Co., Norwood, MA, USA). Geometric factors for sensitivity of crack-based sensor are provided in Supplementary Note 6. Electromyography (PSL-iEMG2, Physiolog. Co., Milton Keynes, UK) measured a muscle response and electrical activity. Flowmeter (5000 Series Digital Flow Meters, TSI. Co., Shoreview, MN, USA) delivered reading a respiration measurement. A digital sound-level meter (TM-101 Sound Level Meter, Tenmars Electronics Co., Taipei, Taiwan) measured the level of sound by the tuning fork. DAQ system (SIRIUS-SYSTEM, DEWESoft Korea. LTD, Anyang, Korea) measured mechanical signals of TUNES.

FEA simulation of TUNES

First, to analyze the mechanical behavior of crack-based sensor at crack interfaces according to the applied strain, we conducted 2D FEA of unit crack (length and thickness are 5 and 7.5 μm) using the ABAQUS. Crack-based sensor consists of 7.5 μm polyimide film and metal layers (50 nm Chromium and 30 nm gold). Since the thickness of the metal layers is very thin compared to polyimide, it can be ignored. Linear tensile stretching analysis was performed to compare the crack depth and crack gap with the experimental value. The initial dimension of crack depth and crack gap of were 5 and 400 nm. One side of the film is fixed, and the other side is applied to 2% tensile strain. Second, to analyze the pressure effect of the pre-strained crack-based sensor, we conducted 3D FEA. The dimensions of crack-based sensor are as follows (length: 30 mm, width: 5 mm, and thickness: 7.5 μm). Linear buckling analysis by pressure effect was performed to analyze the deformation of the length according to the preset strain (0, 0.5, and 1%). The preset strain was applied to both ends of film, and the pressure was generated to the central area (5 mm \times 5 mm). The Polyimide (PI) was set as the linear elastic material with the elastic modulus (E : 2.5 GPa) and Poisson's ratio (ν : 0.34).

Ethical information for studies involving human subjects

Clinical trial of TUNES was conducted under the IRB protocol (IRB No. H-1808-177-969) approved by Seoul National University Hospital Institutional Review Board and clinicalTrials.gov identifier (NCT number) is NCT03805815. Pulse data of 20's men and 70's women in Fig. 5 were measured under the IRB protocol (IRB No. 202208-HB-EX-001) approved by Ajou University Institutional Review Board. All participants submitted the written informed consents and were advised that they could withdraw from the study at any time.

DATA AVAILABILITY

All data are available within the article or available from the authors upon reasonable request.

CODE AVAILABILITY

Code is available within from the authors upon a reasonable request.

Received: 12 October 2022; Accepted: 24 February 2023;

Published online: 09 March 2023

REFERENCES

- Finck, A. The lyriform organ of the orb-weaving spider *Araneus bicinctus*: Vibration sensitivity is altered by bending the leg. *J. Acoust. Soc. Am.* **70**, 231–233 (1981).
- Young, S. L. et al. Micromechanical properties of strain-sensitive lyriform organs of a wandering spider (*Cupiennius salei*). *Acta Biomater.* **41**, 40–51 (2016).
- Barth, F. G. Der sensorische Apparat der Spaltssinnesorgane (*Cupiennius salei* Keys., Araneae). *Z. für Zellforsch. und mikroskopische Anat.* **112**, 212–246 (1971).
- Barth, F. G. & Bohnenberger, J. Lyriform slit sense organ: thresholds and stimulus amplitude ranges in a multi-unit mechanoreceptor. *J. Comp. Physiol.* **125**, 37–43 (1978).
- Speck, J. & Barth, F. G. Vibration sensitivity of pretarsal slit sensilla in the spider leg. *J. Comp. Physiol.* **148**, 187–194 (1982).
- Yamada, T. et al. A stretchable carbon nanotube strain sensor for human-motion detection. *Nat. Nanotechnol.* **6**, 296–301 (2011).
- Kang, D. et al. Ultrasensitive mechanical crack-based sensor inspired by the spider sensory system. *Nature* **516**, 222–226 (2014).
- Schwartz, G. et al. Flexible polymer transistors with high pressure sensitivity for application in electronic skin and health monitoring. *Nat. Commun.* **4**, 1–8 (2013).
- Mannsfeld, S. C. et al. Highly sensitive flexible pressure sensors with microstructured rubber dielectric layers. *Nat. Mater.* **9**, 859–864 (2010).
- Pan, L. et al. An ultra-sensitive resistive pressure sensor based on hollow-sphere microstructure induced elasticity in conducting polymer film. *Nat. Commun.* **5**, 1–8 (2014).
- Zang, Y. et al. Flexible suspended gate organic thin-film transistors for ultra-sensitive pressure detection. *Nat. Commun.* **6**, 1–9 (2015).
- Kim, D.-S. et al. Highly durable crack sensor integrated with silicone rubber cantilever for measuring cardiac contractility. *Nat. Commun.* **11**, 1–13 (2020).
- Roh, Y. et al. Vital signal sensing and manipulation of a microscale organ with a multifunctional soft gripper. *Sci. Robot.* **6**, eab16774 (2021).
- Liu, L. et al. Bioinspired, omnidirectional, and hypersensitive flexible strain sensors. *Adv. Mater.* **34**, 2200823 (2022).
- Wang, S. et al. Skin electronics from scalable fabrication of an intrinsically stretchable transistor array. *Nature* **555**, 83–88 (2018).
- Hua, Q. et al. Skin-inspired highly stretchable and conformable matrix networks for multifunctional sensing. *Nat. Commun.* **9**, 1–11 (2018).
- Araromi, O. A. et al. Ultra-sensitive and resilient compliant strain gauges for soft machines. *Nature* **587**, 219–224 (2020).
- Trung, T. Q. & Lee, N. E. Recent progress on stretchable electronic devices with intrinsically stretchable components. *Adv. Mater.* **29**, 1603167 (2017).
- Kim, D.-H. et al. Epidermal electronics. *Science* **333**, 838–843 (2011).
- Han, M. et al. Three-dimensional piezoelectric polymer microsystems for vibrational energy harvesting, robotic interfaces and biomedical implants. *Nat. Electron.* **2**, 26–35 (2019).
- Miyamoto, A. et al. Inflammation-free, gas-permeable, lightweight, stretchable on-skin electronics with nanomeshes. *Nat. Nanotechnol.* **12**, 907–913 (2017).
- Chung, H. U. et al. Binodal, wireless epidermal electronic systems with in-sensor analytics for neonatal intensive care. *Science* **363**, eaau0780 (2019).
- Kim, J. J. et al. Skin electronics: next-generation device platform for virtual and augmented reality. *Adv. Funct. Mater.* **31**, 2009602 (2021).
- Kim, K. K. et al. A deep-learned skin sensor decoding the epicentral human motions. *Nat. Commun.* **11**, 1–8 (2020).
- Wang, B. et al. Firing frequency maxima of fast-spiking neurons in human, monkey, and mouse neocortex. *Front. Cell. Neurosci.* **10**, 239 (2016).
- Kim, T. et al. Polyimide encapsulation of spider-inspired crack-based sensors for durability improvement. *Appl. Sci.* **8**, 367 (2018).
- Jian, M. et al. Flexible and highly sensitive pressure sensors based on bionic hierarchical structures. *Adv. Funct. Mater.* **27**, 1606066 (2017).
- Yao, H. B. et al. A flexible and highly pressure-sensitive graphene-polyurethane sponge based on fractured microstructure design. *Adv. Mater.* **25**, 6692–6698 (2013).
- Su, B., Gong, S., Ma, Z., Yap, L. W. & Cheng, W. Mimosa-inspired design of a flexible pressure sensor with touch sensitivity. *Small* **11**, 1886–1891 (2015).
- Gong, S. et al. A wearable and highly sensitive pressure sensor with ultrathin gold nanowires. *Nat. Commun.* **5**, 1–8 (2014).
- Yeo, J. C., Yu, J., Koh, Z. M., Wang, Z. & Lim, C. T. Wearable tactile sensor based on flexible microfluidics. *Lab Chip* **16**, 3244–3250 (2016).
- Ai, Y. et al. An ultrasensitive flexible pressure sensor for multimodal wearable electronic skins based on large-scale polystyrene ball@ reduced graphene-oxide core-shell nanoparticles. *J. Mater. Chem. C* **6**, 5514–5520 (2018).
- Li, T. et al. A flexible pressure sensor based on an MXene-textile network structure. *J. Mater. Chem. C* **7**, 1022–1027 (2019).
- Ji, B. et al. Facile preparation of hybrid structure based on mesodome and micropillar arrays as flexible electronic skin with tunable sensitivity and detection range. *ACS Appl. Mater. Interfaces* **11**, 28060–28071 (2019).
- Bae, G. Y. et al. Linearly and highly pressure-sensitive electronic skin based on a bioinspired hierarchical structural array. *Adv. Mater.* **28**, 5300–5306 (2016).
- Lou, Z., Chen, S., Wang, L., Jiang, K. & Shen, G. An ultra-sensitive and rapid response speed graphene pressure sensors for electronic skin and health monitoring. *Nano Energy* **23**, 7–14 (2016).

37. Tortora, G. J. & Derrickson, B. H. *Principles of Anatomy and Physiology* (John Wiley & Sons, 2018).
38. Causey, L., Cowin, S. C. & Weinbaum, S. Quantitative model for predicting lymph formation and muscle compressibility in skeletal muscle during contraction and stretch. *Proc. Natl Acad. Sci. USA* **109**, 9185–9190 (2012).
39. Gennisson, J. L., Cornu, C., Catheline, S., Fink, M. & Portero, P. Human muscle hardness assessment during incremental isometric contraction using transient elastography. *J. Biomech.* **38**, 1543–1550 (2005).
40. Ma, Y. et al. Relation between blood pressure and pulse wave velocity for human arteries. *Proc. Natl Acad. Sci. USA* **115**, 11144–11149 (2018).
41. de Vecchi, A. et al. Catheter-induced errors in pressure measurements in vessels: an in-vitro and numerical study. *IEEE Trans. Biomed. Eng.* **61**, 1844–1850 (2014).
42. Marik, P. E., Monnet, X. & Teboul, J.-L. Hemodynamic parameters to guide fluid therapy. *Ann. Intensive Care* **1**, 1–9 (2011).
43. Rajendra Acharya, U., Paul Joseph, K., Kannathal, N., Lim, C. M. & Suri, J. S. Heart rate variability: a review. *Med. Biol. Eng. Comput.* **44**, 1031–1051 (2006).
44. Froelicher, V. F. Jr et al. Prediction of maximal oxygen consumption: comparison of the Bruce and Balke treadmill protocols. *CHEST* **68**, 331–336 (1975).
45. Polson, N. G. & Scott, S. L. Data augmentation for support vector machines. *Bayesian Anal.* **6**, 1–23 (2011).
46. Liaw, A. & Wiener, M. Classification and regression by randomForest. *R. N.* **2**, 18–22 (2002).

ACKNOWLEDGEMENTS

We thank Junggon Kim for discussion of biomimetic of spider's tuning ability. This work is supported by funding from NRF of Korea (grant no. 2019R1H1A1080221, 2019R1F1A1063066, 2019R1C1C1007629, 2021R1A6A3A01087289, 2021R1A6A3A13045869, 2022R1A2C2093100, 2022R1A6A3A13071489). The new faculty research fund of Ajou University, and the Ajou University research fund. This work was supported by Korea Environment Industry & Technology Institute (KEITI) through Digital Infrastructure Building Project for Monitoring, Surveying, and Evaluating the Environmental Health Program, funded by Korea Ministry of Environment (MOE) (2021003330009). This research was supported by a grant of the Basic Research Program funded by the Korea Institute of Machinery and Materials (grant number: NK231A).

AUTHOR CONTRIBUTIONS

T.K., I.H. and Y.R. contributed equally to this work; T.K. led the work; I.H. and Y.R. designed the experiments; S.K. and S.L. programmed machine learning algorithm; S.J.,

C.K. and D.K. performed the device characterization; K.J. performed Bluetooth setup; J.L., G.L., S.K. and M.K. performed signal processing; D.G. performed FEA simulation; J.P. and S.S. performed data collection; K.A. performed sensor fabrication; H.S.L., J.K., B.K.K. and J.M.H. performed clinical trial; B.K.K., J.K., S.H. and D.K. supervised the project.

COMPETING INTERESTS

The authors declare no competing interests.

ADDITIONAL INFORMATION

Supplementary information The online version contains supplementary material available at <https://doi.org/10.1038/s41528-023-00247-2>.

Correspondence and requests for materials should be addressed to Bon-Kwon Koo, Je-sung Koh, Seungyong Han or Daeshik Kang.

Reprints and permission information is available at <http://www.nature.com/reprints>

Publisher's note Springer Nature remains neutral with regard to jurisdictional claims in published maps and institutional affiliations.



Open Access This article is licensed under a Creative Commons Attribution 4.0 International License, which permits use, sharing, adaptation, distribution and reproduction in any medium or format, as long as you give appropriate credit to the original author(s) and the source, provide a link to the Creative Commons license, and indicate if changes were made. The images or other third party material in this article are included in the article's Creative Commons license, unless indicated otherwise in a credit line to the material. If material is not included in the article's Creative Commons license and your intended use is not permitted by statutory regulation or exceeds the permitted use, you will need to obtain permission directly from the copyright holder. To view a copy of this license, visit <http://creativecommons.org/licenses/by/4.0/>.

© The Author(s) 2023